Shear stress induced lipid order and permeability changes of giant unilamellar vesicles

Nicolas Färber [a,b], Jonas Reitler [b], Andrej Kamenac [a], Christoph Westerhausen [a,b,c,*]

[a] Experimental Physics I, Institute of Physics, University of Augsburg, Universitätsstr. 1, 86159 Augsburg, Germany
[b] Physiology, Institute of Theoretical Medicine, University of Augsburg, Universitätsstraße 2, 86159 Augsburg, Germany
[c] Center for NanoScience (CeNS), Ludwig-Maximilians-Universität Munich, 80799 Munich, Germany

1. Introduction

The encapsulation of drugs in liposomes allows for targeted release of therapeutic substances to treat locally diseased tissue by exploiting the dependency of the lipid membrane permeability on external stimuli such as pH, redox-potential, light illumination, magnetic fields, temperature and shear stress [1–6]. In the case of temperature-sensitive liposomes the lipid composition is adjusted in a way that the system is close to a phase transition between an ordered and disordered lipid state. A slight variation of temperature can therefore cause a shift of the lipid system into the phase transition regime where membrane area fluctuations and the lipid membrane compressibility are strongly increased. By this the formation of pores is facilitated causing the membrane permeability to increase [7,8]. The main phase transition or melting temperature T_m between the ordered or gel-like and the disordered or fluid lipid phases depends aside from the composition of lipid species on thermodynamic variables such as pressure, pH, electric field and salt concentration [9–12]. In this context we want to focus on shear stress as another parameter that influences the membrane state of liposomes. As vesicles deform under shear flow and deformation increases the lipid bilayer tension we assume that in turn the lipid order decreases. The same effect was observed for increased membrane tension induced by vesicle swelling [13–15]. Therefore, we expect a decreased melting temperature of liposomes under shear exposure and in consequence an increased membrane permeability at temperatures below the static melting temperature T_m. Additionally, lipid membrane permeability could be enhanced independent of the phase state by mere mechanical forces inducing pore formation. To elucidate how temperature and shear stress interdependently affect the quantities membrane permeability and lipid order, in this study, we conducted experiments

* Corresponding author at: Experimental Physics I, Institute of Physics, University of Augsburg, Universitätsstr. 1, 86159 Augsburg, Germany.
E-mail address: christoph.westerhausen@gmail.com (C. Westerhausen).

using giant unilamellar vesicles (GUVs) labelled with different probes: The permeability was determined by the loss of fluorescently labelled dextran of initially fully loaded GUVs using fluorescence microscopy (Fig. 1b) after shear exposure in a polyethylene (PE) tube at different temperatures (Fig. 1a). The temperature and shear stress induced lipid order changes of GUVs labelled with the membrane-embedded probe Laurdan were analyzed in situ in a glass capillary by spectral decomposition. The emission spectrum of Laurdan being sensitive to the polarity and relaxation dynamics of its surrounding indicates a lipid order change from gel to fluid lipid state by a shift of the maximum fluorescence intensity from 440 nm (blue) to 490 nm (greenish) [16,17]. To quantify the degree of lipid order, we used the generalized polarization

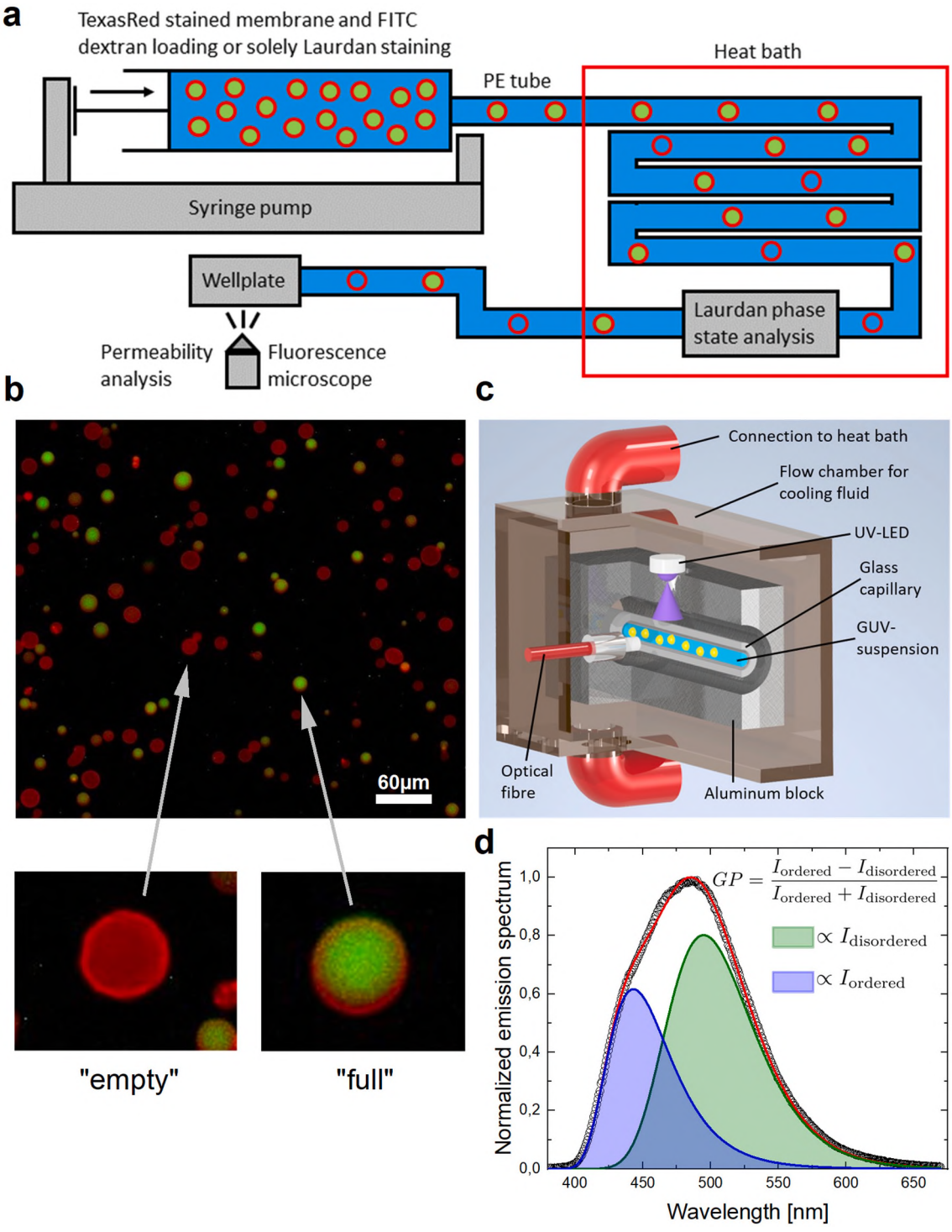

Fig. 1. Experimental setup and data analysis. a Giant unilamellar vesicles were exposed to shear flow in a PE-tube at different flow rates and temperatures. **b** After shear exposure the TexasRed stained GUV membranes were detected by fluorescence microscopy and the loss of FITC dextran was determined as a measure of permeability. The micrographs indicate that near the phase transition temperature T_m the GUV membrane permeability follows an all-or-nothing behavior. **c** The lipid order of GUVs exclusively stained with Laurdan was analyzed in situ under shear flow in a glass capillary. The membrane order probe Laurdan was excited by an UV-LED and the emission spectra were recorded by an optical fiber attached to a spectrometer. **d** The recorded spectra were analyzed by approximation with two lognormal functions which allowed for determination of GP.

GP, as defined in the M&M section, that approaches GP = 1 when the lipid membrane is fully ordered in the gel phase and GP = -1 for a completely disordered membrane in the fluid phase [18]. We determined the blue and green intensities of the Laurdan emission spectrum by approximation with two lognormal functions (Fig. 1c) as proposed by Bacalum et al. [19]. Because of channel cross talk between Laurdan and fluoresceinisothiocyanat-dextran (FITC-dextran) we analyzed the quantities permeability and membrane order separately.

Our study was designed as follows: First, we analyze the permeability of GUVs as function of temperature and shear force around the static lipid melting temperature. Second, we investigate whether permeability changes induced at the phase transition are dependent of the direction in which the phase transition is crossed (from gel to fluid and vice versa). Third, we examine the lipid order changes induced by shear force to quantify to which extend the permeability is affected by shear force induced lipid order changes. At last, we compare the permeability measurements recorded near the melting temperature with a lipid system being far in the fluid phase to prove that the permeability changes observed before are a result of the proximity to the phase transition regime.

2. Materials and methods

Fluorescence microscopy was performed using a Zeiss Axiovert 200 M (Carl Zeiss AG, Germany) epi-fluorescence microscope. Giant unilamellar vesicle membranes stained with Texas Red™ 1,2-Dihexadecanoyl-sn-Glycerin-3-Phospho-ethanolamin (Thermo Fisher Scientific, Germany) were imaged with 585/30 nm and 625/40 nm excitation/emission bandpass filters. For vesicle content analysis of FITC-dextran (Sigma-Aldrich Chemie GmbH, Germany) we used 470/20 nm and 510/40 nm as excitation/emission wavelengths.

Spectrum acquisition for phase state analysis of Laurdan (Sigma-Aldrich Chemie GmbH, Germany) stained giant unilamellar vesicles under shear flow was performed using an Ocean optics QEPro spectrometer (Ocean Optics Germany GmbH, Germany) and an optical fiber connected to the custom-made temperature control setup that is depicted in Fig. 1c. The vesicles were excited using a 360 nm LED with UV-bandpass in a glass capillary embedded in a temperature-controlled aluminum block. The emitted light was captured after an UV-band-stop-filter by the optical fiber without any focusing optical elements.

Giant unilamellar vesicles were prepared by electroformation [20]: For GUV permeability analysis lipids (Avanti Polar lipids, AL, USA) dissolved in chloroform were mixed with 1 mol% Texas Red™ 1,2-Dihexadecanoyl-sn-Glycero3-Phospho-ethanolamine, Triethylammonium Salt (TexasRed) and dried on fluorine tin oxide (FTO)-coated glass slides under vacuum for at least 60 min. Afterwards a 100 mM glucose 5 μM FITC-dextran (MW = 10^4 g/mol) water solution was filled between two FTO-coated glass slides separated by a Teflon spacer. A rectangular 10 Hz AC voltage was applied to induce vesicle formation. After initial 15 min the applied electric field was increased from 0.6 to 2.4 V/mm. The temperature during vesicle formation was kept 15 K above the lipid melting transition temperature. For shear force dependent phase state analysis, we used a Laurdan (Sigma-Aldrich Chemie GmbH, Munich, Germany) concentration of 16 mol% and a 100 mM glucose solution without FITC-dextran to avoid channel crosstalk.

Differential scanning calorimetry (DSC) was performed with a MicroCal VP-DSC calorimeter (MicroCal Inc., now Malvern Panalytical Ltd., UK). GUVs were analyzed in degassed saccharose solution at 15 psi pressure with a scan rate of 15 K/h and saccharose solution as reference. The up-scan after three subsequent measurement cycles was used for data analysis and corrected by baseline subtraction as described previously [21].

Shear flow was created in a polyethylene tube of $R = 190$ μm inner radius using a Harvard PHD 2000 Infusion syringe pump. The experiments were conducted at different flow rates of Q = 0.1, 0.2, 0.5, 2, 10 and 50 ml/h which induce position dependent shear velocities $\dot{\gamma} = \frac{dv}{dr} = 4\frac{\dot{V}}{R^4}\frac{r}{\pi}$ where r is the radial distance to the tube center. The shear velocities range from 0 s^{-1} in the tube's center to 5, 10, 26, 103, 516 and 2578 s^{-1} at the tube's boarder. Prior to shear flow exposure the FITC-Dextran background intensity of the GUV suspension was diluted 20-fold by addition of equimolar saccharose solution followed by centrifugation for 10 min at 100 G and supernatant removal. After three repetitions of this washing procedure the GUV suspension was pumped through the tempered tube and collected in a 96-wellplate. After 2 h of sedimentation at 7 °C the samples were imaged with a fluorescence microscope.

Image analysis was performed using Fiji [22] and the stitching plugin of Preibisch et al. [23] followed by threshold based segmentation of the TexasRed-images. After background correction of the FITC-channel images using dark pixel values of GUV free areas the mean FITC intensities within the GUV membranes were determined and normalized to the according vesicle size.

Laurdan emission spectra were automatically fitted using two lognormal functions as proposed by Bacalum et al. [19] within a python script. The generalized polarization defined by Parasassi et al. [18] $GP = \frac{I_{440}-I_{490}}{I_{440}+I_{490}}$ was calculated by using the areas under the two fit functions as values for I_{440} and I_{490}.

3. Results and discussion

We analyzed the permeability of GUVs synthesized using the phospholipids 14:0PC (T_m = 23.5 °C) and 15:0PC (T_m = 34.5 °C) in a temperature range from T = 21 °C to T = 37 °C to cover the gel phase, the fluid phase and the melting regime for both lipid species. To examine whether the observed effects are a result of shear force induced lipid order changes, we recorded the emission spectra of Laurdan stained GUVs at different temperatures and flow rates. Lastly, we investigated the permeability of GUVs consisting of DOPC ($T_m = -18$ °C) being far in the fluid phase at room temperature (23 °C) [24,25] to clarify whether the observed behavior of 14:0PC and 15:0PC GUVs is caused by the proximity to the melting temperature.

3.1. Shear flow dependent permeability near the phase transition

The membrane permeability was analyzed by determining the loss of fluorescence intensity after shear force exposure of GUVs that were initially loaded with FITC dextran. The result of the intensity analysis after a shear force exposure of $\dot{\gamma}_{max}$= 516 s^{-1} at different temperatures above and below the melting point T_m = 34,5 °C of 15:0PC GUVs is shown in Fig. 2a. After passing the tube in the gel phase at 29 °C most of the GUVs kept their FITC dextran content and thus emit a high fluorescence intensity. At 34 °C as the temperature approaches the melting point a second peak located at lower values emerges in the intensity distribution corresponding to GUVs that were permeabilized and in consequence lost their cargo. Above the phase transition at 35 °C the low intensity fraction is even greater than the number of GUVs that contained the FITC dextran and at 37 °C nearly all vesicles lost their cargo. The remarkable observation is that in all scenarios there is no fraction between the two intensity levels meaning that the permeabilization shows an all-or-nothing behavior. This is in agreement with the findings of other research groups who found increased permeability of phospholipid vesicles at the phase transition which is attributed by Blicher et al. to pore formation due to increased membrane compressibility and area fluctuations in the transition regime [8,26,27]. Under static conditions such thermally induced pores exhibit sizes in a range between 0.8 nm and 1.6 nm and should therefore not enable dye leakage of FITC-dextran with a hydrodynamic radius of about 2.3 nm [8,28]. However, if GUVs are exposed to external forces such as electric fields or mechanical stretching even macroscopic pores of few μm can develop and reseal. A recent simulation study shows that the proximity to a phase transition

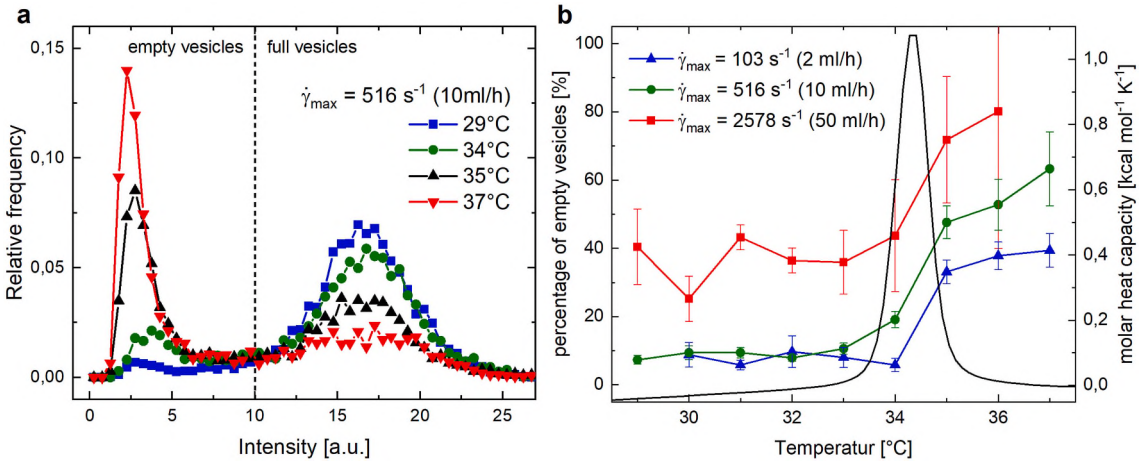

Fig. 2. Shear force and temperature dependent GUV permeability. a FITC dextran intensity distribution of GUVs after passing the PE-tube at 10 ml/h corresponding to a maximum shear rate of 516 s^{-1} at different temperatures. Below the phase transition temperature of $T_m = 34.5$ °C most of the GUVs exhibit a high fluorescence intensity meaning that no loss of FITC dextran due to permeabilization during shear exposure did occur. Above the melting point the fraction of GUVs with low intensity increases meaning that they lost cargo during the treatment. The dotted line between the two populations indicates a threshold value used to calculate the percentage of empty vesicles as a measure for permeabilization of the whole vesicle ensemble. For each histogram about 3000 GUVs were analyzed. **b** Percentage of empty vesicles after shear flow exposure at different temperatures and flow rates. As the GUVs cross the phase transition temperature indicated by the peak in the heat capacity profile measured by DSC the permeability increases. Shear stress affects membrane permeability differently in the gel and fluid phase. The data shown corresponds to three independently conducted experiments. In every experiment about 20,000 vesicles were analyzed. The error bars indicate the deviation of the percentage of empty vesicles upon a 5% increase/decrease of the threshold value.

destabilizes the membrane thus enhancing the effect of external forces as induced by electric fields [29]. We assume that the pore formation mechanism in our study is mediated by an interplay between phase state and shear forces yielding pores larger than 2.3 nm. In our experiment this would mean that once pores are formed within the membrane, they allow the release of cargo until nearly all FITC dextran is lost. In contrast to static experiments, we observe that two subpopulations of GUVs behave completely different even though they are exposed to the same temperature profile. Therefore, the differences in permeability must arise from variations of shear forces during travelling through the PE-tube. GUVs that are located near the tube's center experience lower shear forces than vesicles that travel near the tube's wall. The question whether the shear forces affect the membrane phase state and then in consequence the permeability or if they influence the permeability directly is discussed in the second section.

By defining a threshold as illustrated in Fig. 2a, we can discriminate between two classes of GUVs: vesicles with high fluorescence intensity are referred to as “full” whereas vesicles that were permeabilized and lost their FITC dextran cargo are classified as “empty”. Using this terminology, we can quantify the degree of vesicle permeabilization by the percentage of empty vesicles which is shown in Fig. 2b as function of temperature for three different flow rates. Below 34.5 °C in the gel phase, there is no visible change of permeability when the flow rate is enhanced from Q = 2 ml/h to Q = 10 ml/h in contrast to the fluid phase above $T = 34.5$ °C where permeability is enhanced by a factor of up to 60% at $T = 37$ °C. The increase from a flow rate of 2 ml/h (103 s^{-1}) to 10 ml/h (516 s^{-1}) corresponds to a transition from venous flow conditions (1-6 dyn/cm^2 ~ 36–214 s^{-1}) to an arterial vessel system (10-70 dyn/cm^2 ~ 357–2500 s^{-1}) [30]. Therefore, the permeability dependence of such fluid phase liposomes allows for targeting of different physiological blood flow regimes. Based on these results, we conclude that pore formation during shear exposure is more likely in the fluid phase which can be attributed to the lower bending rigidity and higher area compressibility as compared to the gel phase. At an even higher flowrate of Q = 50 ml/h corresponding to ($\dot{\gamma}$ = 2578 s^{-1}) at the tube's wall the permeability in both phases is enhanced meaning that a distinct threshold of mechanical force has to be overcome in the gel phase to induce pore formation. Such high shear rates simulate the pathological condition of stenosed arterial vessels (>2500 s^{-1} [31]) which could reduce the specificity of thermo-responsive drug carriers as they induce drug release even below the melting temperature. Furthermore, we observed that under these high flow conditions the vesicle size distribution is decreased in the fluid phase (SI Fig. 2) which could indicate that vesicle division or disruption is induced. At lower flow rates however the size distribution is not that much affected. Independent of the flowrate we observe an increase in GUV permeability above the phase transition. This is in contrast to static experiments, where only right at the phase transition a permeability peak was reported. This observation could be attributed to our experimental design. The FITC dextran loaded 15:0PC GUVs were pumped at room temperature being in the gel phase into the tempered tube and in the following collected in a well plate again at room temperature. Therefore, whenever the tube temperature was adjusted to temperatures above the phase transition temperature the GUVs experienced two phase state changes: At first from the gel phase to the fluid phase during warming up and vice versa afterwards during cooling. This is why we think that the increased permeability in the fluid phase is a result of pores that formed at the phase transition and are even stable for a certain time when the membrane is not in the transition, but in the fluid regime.

To test this hypothesis, we analyzed whether GUVs that were at room temperature in the fluid phase would exhibit increased permeability as well when crossing the transition temperature in the other direction when entering the tube that is cooled below the transition temperature. We achieved this by conducting experiments with 14:0PC GUVs that have a transition temperature of $T = 23.5$ °C and are therefore in the fluid phase at an elevated room temperature of $T = 25$ °C. Fig. 3b shows the permeability of vesicles that were pumped with a flowrate of Q = 10 ml/h through the tube that was tempered to 21 °C and 25 °C. The GUVs treated at $T = 21$ °C always remained above the transition temperature T_m in the fluid phase and were less permeabilized than the vesicle ensemble that crossed T_m. For this comparison, we analyzed in addition to the empty vesicle percentage the mean fluorescence intensity as well. In case of low intensity this measure indicates a high degree of permeabilization. For both quantities, we compared the shear exposed samples with a reference that was as well centrifuged for background reduction and kept at room temperature for the same time interval as the shear exposure. As the fraction of empty vesicles is increased by 15 percentage points and the mean fluorescence is decreased by 5

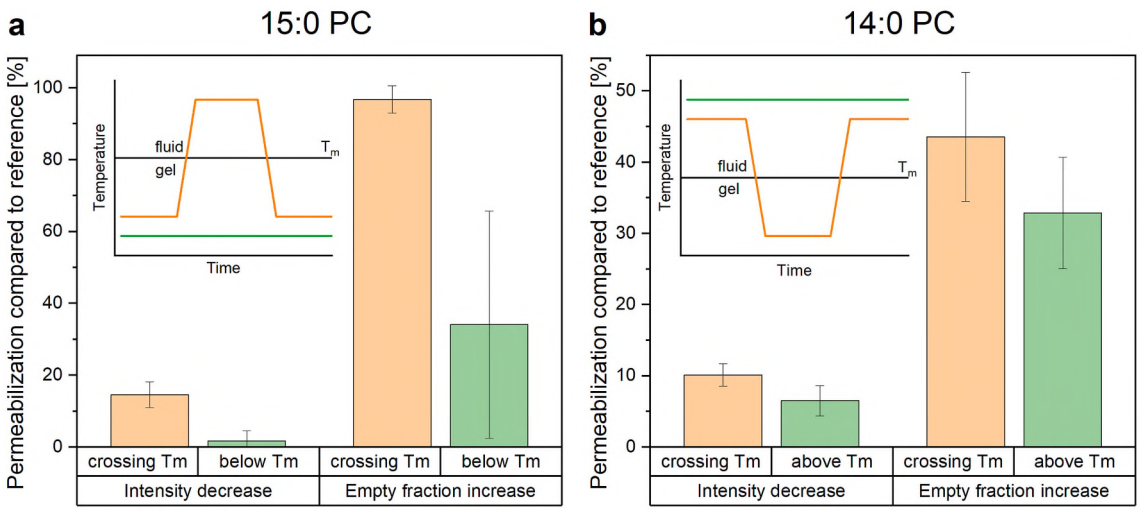

Fig. 3. GUV permeability after shear exposure solely in the fluid or gel phase and after crossing the phase transition in different directions. a Two measures of permeability of 15:0 PC GUVs exposed to shear flow at temperatures below and above the melting transition. As the 15:0PC GUVs are before and after treatment in the gel state at room temperature their phase state as function of time is either always the gel state or they change to the fluid phase for the time in the tube. The permeability measured either by the mean FITC dextran intensity loss or by the increase of the number of empty vesicles show is enhanced in case of crossing the phase transition. **b** 14:0 PC GUVs were at a room temperature of 25 °C before and after the treatment in the fluid phase. In case of shear flow exposure at 25 °C they stayed always in the fluid phase and at 21 °C tube temperature they changed to the gel state for the time of shear exposure. The permeability of GUVs crossing the phase transition is again increased compared to GUVs undergoing no phase state change. Error bars indicate the standard deviation of three independently conducted experiments. At least 2000 vesicles were analyzed to determine the mean value of a single experiment.

percentage points both measures confirm our hypothesis that the increased permeability is a result of crossing the phase transition temperature. However, the effect for 15:0PC samples is less pronounced. We attribute this to closer proximity of the temperature to T_m for 14:0PC samples.

As the permeability of 14:0PC GUVs (Fig. 3b) that remained in the fluid phase and 15:0PC vesicles (Fig. 3a) in the gel phase is in both cases reduced compared to the case of crossing the phase transition we conclude that the membrane permeability is highest right at the melting temperature and the obtained step-like permeability as function of temperature is a result of our experimental setup.

3.2. *Shear flow effects on the lipid membrane phase state*

The divergence of the permeability of GUVs under shear flow in a way that some vesicles are completely permeabilized and others show nearly no loss of cargo (Fig. 1b and Fig. 2a) raises the question by which mechanism shear forces affect the lipid membrane state. Two scenarios seem plausible: Either the mechanical forces during vesicle deformation directly open up pores within the membrane, or the shear force itself acts as a thermodynamic variable that shifts the phase state of the lipid membrane towards the phase transition where the permeability is high due to the increased area compressibility and increased fluctuations. To encounter this problem, we used the setup already shown in Fig. 1c that allows us to analyze the emission spectra of Laurdan stained GUVs under shear flow at various temperatures. The fluorescence analysis yields the generalized polarization as a measure for the lipid chain order that can vary between GP = -1 meaning all lipids are in the fluid state and GP = 1 where all lipids are in the gel state. The GP value of 15:0PC as a function of temperature is shown in Fig. 4a for three different flow rates and a static reference.

The phase transition between the gel and fluid phase manifests as steep decrease of the GP value around $T = 33$ °C. The derivative of GP with respect to temperature shown in Fig. 4b yields a quantity that behaves like the excess heat capacity and exhibits a peak at the phase transition temperature T_m. The shift of $T_{m,GP}$ by $\Delta T = 1.1$ K relative to $T_{m,DSC}$ is a result of melting point depression due to a low lipid to probe ratio (7:1) which was necessary to achieve an assessable Laurdan signal in the glass capillary where the measurement took place. The Laurdan spectra recorded under shear exposure of Q = 0.1, 0.2 and 0.5 ml/h show a reversible red shift meaning that directly after stopping the flow the spectra returned to its initial shape under static conditions. This reversible spectral shift is visible in Fig. 4a as lowering of the GP value at constant temperature with increasing flow rate and as left shift of the dGP/dT profiles in Fig. 4b. The maximum of the dGP/dT graphs indicating the melting temperature T_m under flow is plotted as function of temperature in Fig. 4e and yields that there is a maximum reversible shift of the melting transition of $\Delta T = -0.3$ K, meaning that shear forces lower the lipid chain order of GUVs. This observation supports the hypothesis that near phase transitions shear flow changes the GUV membrane's phase state rendering it more fluid and by this affecting the membrane's permeability. Similar effects were observed for mechanical strain induced by osmotic swelling in Laurdan stained vesicles: With increasing strain and also for increasing membrane curvature a drop of the GP value was measured [15]. Higher strain and higher curvature favor the lipid phase state with lower bending rigidity and larger membrane area, namely the fluid phase.

The flow rates discussed so far are much lower than the ones used for the FITC dextran permeability analysis. The spectral change of the Laurdan emission induced by a flowrate as used for the permeability analysis at 10 ml/h exhibits two remarkable differences: The spectral shift is directed towards lower wavelengths, and it is not reversible meaning that after turning off the shear flow the GUVs remained in this state. The spectral change leads to increased GP values (Fig. 4c) and a shift of the melting transition towards higher temperatures (Fig. 4d). The maximal transition shift of $\Delta T = 0.7$ K was observed at a flowrate of Q = 50 ml/h and is shown together with Q = 10 ml/h as red data points in Fig. 4e indicating that these shifts were irreversible. Because of the irreversibility in combination with a loss of overall Laurdan intensity (SI-Fig. 1) during the shear exposure, we think that membrane-embedded Laurdan is lost due to shear forces and the effect of the melting point depression is reduced leading to a detected phase state change in the direction of the Laurdan free GUVs that we measured by DSC (Fig. 4d).

As expected and described in the introduction we observed a reversible shift of the melting temperature T_m under shear flow by

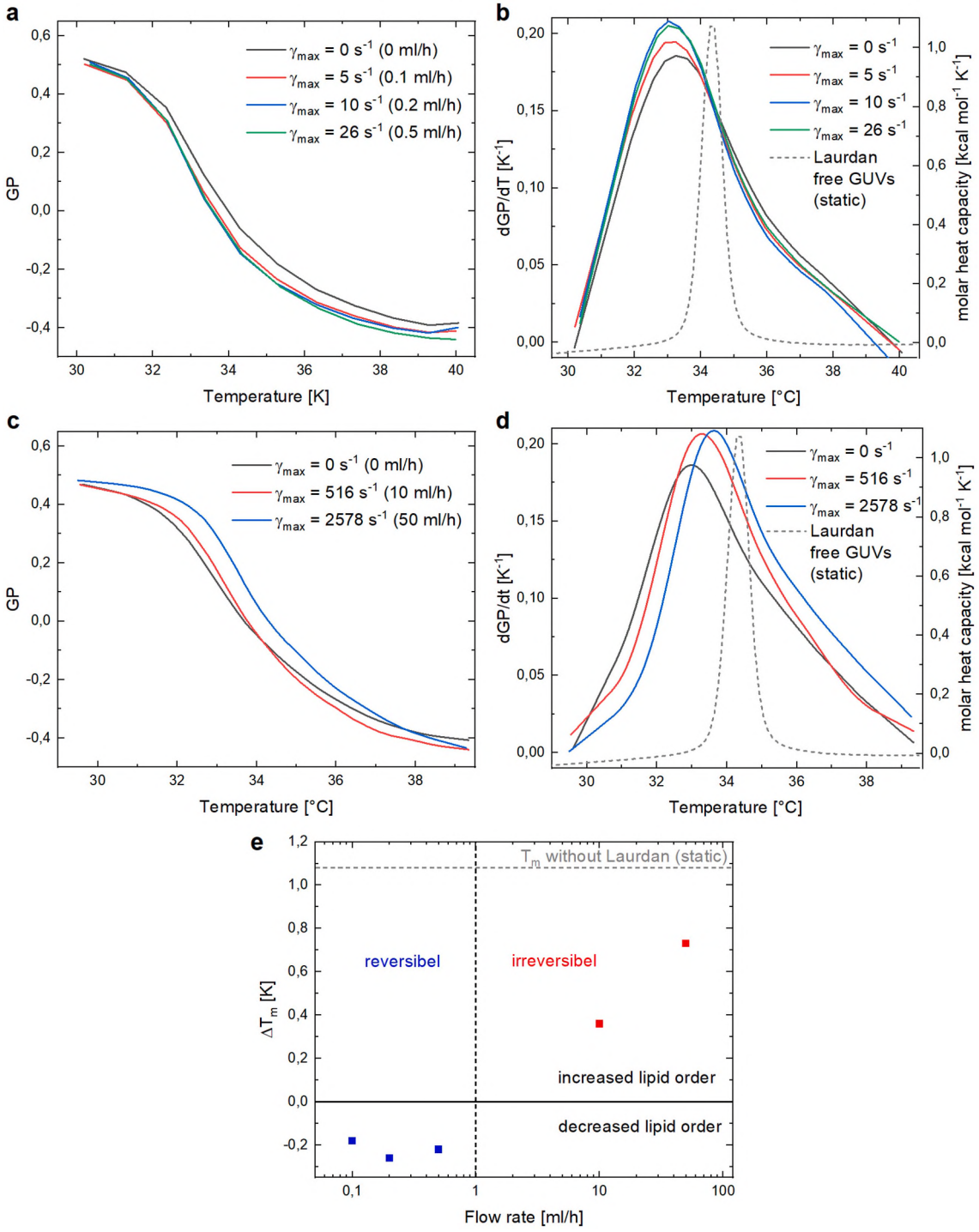

Fig. 4. Membrane order analysis of Laurdan stained 15:0 PC GUVs at varying temperatures and flow rates. a GP temperature profiles determined by spectral analysis as shown in Fig. 1d recorded at different flow rates. The membrane phase transition from the gel to fluid state manifests itself in a steep decrease of GP. With increasing shear forces GP decreases reversibly meaning a decreased order of the GUV membranes. **b** The negative derivative of GP with respect to temperature indicates the phase transition temperature T_m as a peak. The high probe to lipid ratio causes a melting point reduction compared to the label free sample measured by DSC (dotted line). T_m shifts reversibly to lower temperatures with increasing shear force. **c** GP profiles of GUVS exposed to higher flow rates than in a. GP increases irreversibly due to shear exposure. **d** The optically determined melting point Tm is shifted irreversibly to higher temperatures towards the label free reference. **e** Optically determined melting temperatures of 15:0PC GUVs as function of flow rate. Low flow rates cause a reversible fluidization of the lipid membrane while high shear forces change the phase state irreversible and shift T_m towards the label free transition temperature.

optical analysis of Laurdan stained GUVs. At comparatively low flow rates, T_m is decreases by −0.3 K meaning an expansion of the fluid phase. As the loss of membrane embedded Laurdan at high flow rates leads to an irreversible melting point shift of maximal 1.1 K towards the label free sample measured under static conditions, we can estimate that even at the highest flow rates the shear force induced melting temperature shift does not exceed $\Delta T = -1.1$ K. As we observed the all-or-nothing permeability behavior in a range of 5 K around the phase transition temperature (Fig. 2b), we conclude that shear force induced lipid order changes play a minor role during the permeabilization

process. A scenario in which shear forces directly induce membrane pores that possess relatively long pore lifetimes due to the proximity to the phase transition seems to be more likely. To further support this hypothesis, in the following we investigate GUVs far off the melting temperature.

3.3. Shear flow dependent permeability far off the phase transition

The observed all-or-nothing permeability behavior of GUVs under shear flow suggests that there is a non-linear response of the pore-formation likelihood to mechanical shear forces. This might be a result of the proximity to the phase transition where physical properties of lipid membranes tend to change strongly as function of thermodynamic variables such as temperature, pressure and pH. To examine this assumption, we conducted experiments with DOPC that exhibits the main phase transition at a temperature of $T_m = -18$ °C facilitating experiments with GUVs far in the fluid phase at room temperature. The fluorescence intensities of a reference sample that was not exposed to shear flow and two GUV ensembles that were pumped through the tube with a flow rate of Q = 10 ml/h and Q = 50 ml/h at a temperature of $T = 23$ °C are shown in Fig. 5a. Even though the shift of the intensity distribution towards lower values clearly indicates an increased permeability by shear exposure, there is no split of the vesicle population in completely permeabilized and nearly unaffected GUVs as we observed it in Fig. 2a for 15:0PC. The fluorescence micrographs shown in Fig. 5c strongly support this statement as in case of 15:0PC the vesicles can easily be classified in "full" and "empty" by eye and the DOPC GUV FITC dextran intensity seems to be homogeneous (Fig. 5d). Because of this continuous shift of the intensity distribution the definition of an intensity threshold value is neither obvious nor helpful and therefore we compared only the mean FITC dextran intensity of the shear exposed samples to the reference in Fig. 5b. The analysis yields a decrease in fluorescence intensity by 18% at Q = 10 ml/h and 25% for Q = 50 ml/h.

The DOPC GUV experiments suggest that even far off the phase transition shear forces permeabilize the lipid membrane, but the mechanism is different to the permeabilization near a phase transition as in the first case the whole ensemble is affected homogenously and in the second case only a fraction of GUVs is influenced.

4. Conclusion

We have demonstrated that independent of the direction in which a phase transition is passed, GUV permeability is enhanced compared to the case that the membrane stays always in the fluid or the gel state.

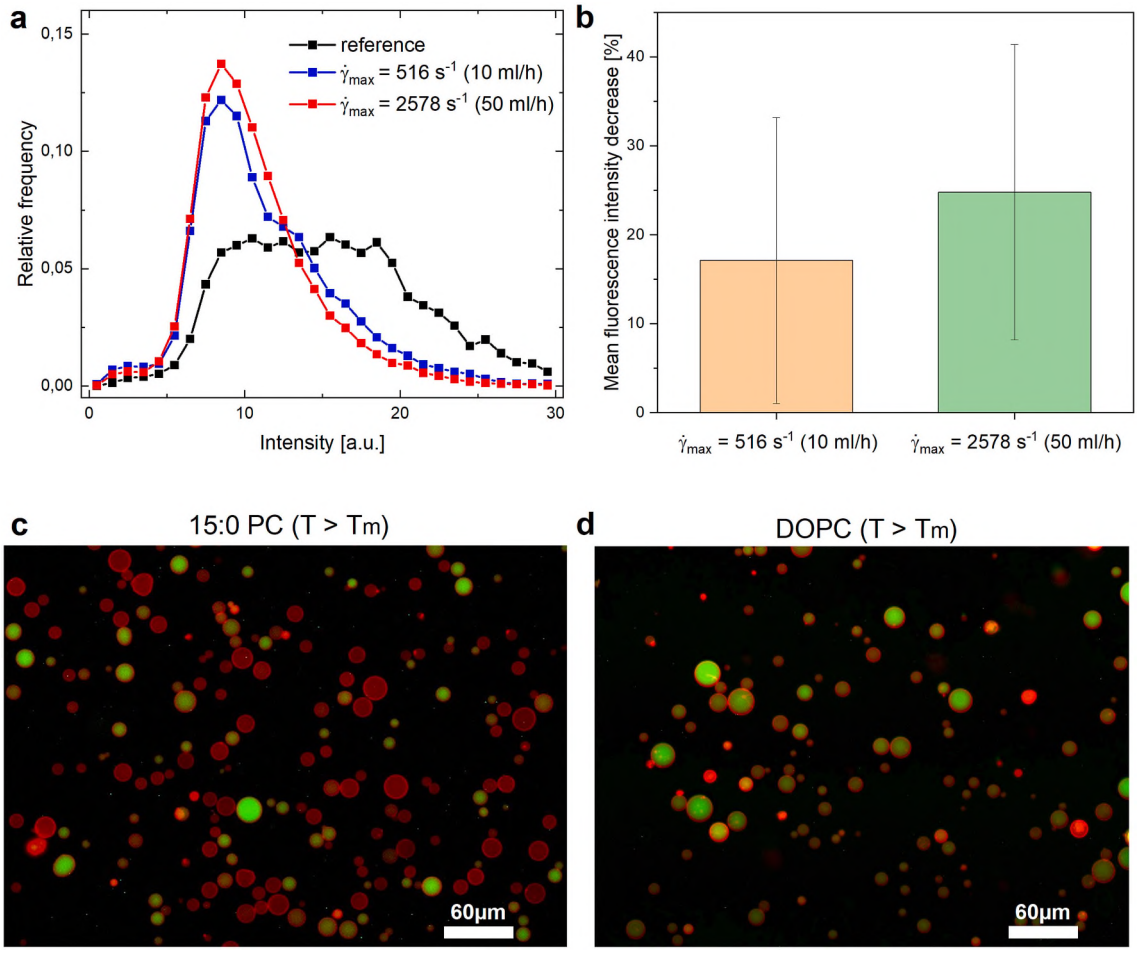

Fig. 5. Membrane permeability of DOPC GUVs under varying shear forces. a Intensity distribution of DOPC GUVs after shear flow exposure at Q = 10 and Q = 50 ml/h corresponding to a wall shear velocity of $\dot{\gamma} = 516$ and $\dot{\gamma} = 2578$ s^{-1} at room temperature. In contrast to GUVs that were exposed to shear flow near their melting point in Fig. 2a the DOPC FITC dextran intensities do not show the formation of two populations but a gradual shift of intensities to lower values with increasing shear flow. **b** The intensity decrease compared to the reference sample as measure for vesicle permeabilization shows increasing permeability with increasing shear force. The quantity of empty vesicles as used before is not suited for DOPC as a uniform permeabilization of the vesicle ensemble is induced. **c, d** Fluorescence micrographs of 15:PC GUVs exposed to shear flow near the phase transition temperature in the fluid phase and DOPC GUVs after the same shear force treatment in the fluid phase but further away from the melting point. While in the case of 15:0PC some vesicles lose all of their cargo and some stay almost unaffected, the DOPC GUVs show a uniform distribution of intensities.

Near the melting temperature GUVs show an all-or-nothing permeability behavior under shear flow meaning that they stay either unaffected or lose all their cargo. Optically measured reversible lipid order changes suggest that shear flow decreases lipid order and acts as a thermodynamic force that reduces the melting temperature. However, the effect strength is less than $\Delta T = -1.1$ K and cannot not explain the diverging permeability within one GUV sample. Shear forces seem to directly induce membrane pores whose lifetimes are enhanced near the phase transition as compared to the case far off the transition temperature as the DOPC permeability measurements suggest.

Our study suggests that even though the shear force induced melting temperature shift is small it must be taken into consideration when thermo-responsive liposomes are designed that will experience high shear exposure in constricted vessels and regions of high flow rates. In addition, our findings can help to understand the release mechanism of thermo-responsive drug carriers: The release of cargo is predicted to be quantized and not continuous.

Data availability

All data that support our findings are available from the corresponding authors upon reasonable request. There are no restrictions on data availability.

Author contributions

N.F., A.K. and C.W. designed research; N.F., J.R. and C.W. performed research; N.F. analyzed data and implemented experimental tools; N.F. and C.W. wrote the paper.

CRediT authorship contribution statement

Nicolas Färber: Investigation, Conceptualization, Methodology, Software, Data curation, Writing – original draft. **Jonas Reitler:** Investigation, Methodology, Software, Data curation, Writing – review & editing. **Andrej Kamenac:** Investigation, Methodology, Writing – review & editing. **Christoph Westerhausen:** Conceptualization, Methodology, Writing – original draft, Writing – review & editing, Supervision.

Declaration of Competing Interest

The authors declare no competing interests.

Data availability

Data will be made available on request.

Acknowledgements

The authors thank Matthias Schneider, Simon Fabiunke and Achim Wixforth for fruitful discussions. The authors thank the Center for Nanoscience (CeNS) and the Augsburg Centre for Innovative Technologies (ACIT) for funding. C.W. would like to acknowledge funding for the project “Physical and functional interaction mechanisms at cell membranes and vessel walls” by the University of Augsburg. N.F. and A. K. would like to thank the Joachim Herz foundation.

Appendix A. Supplementary data

Supplementary data to this article can be found online at https://doi.org/10.1016/j.bbagen.2022.130199.

References

[1] D.S. dos Ferreira, S.C.A. de Lopes, M.S. Franco, M.C. Oliveira, pH-sensitive liposomes for drug delivery in cancer treatment, Ther. Deliv. 4 (2013) 1099–1123.
[2] H. Fu, K. Shi, G. Hu, Y. Yang, Q. Kuang, L. Lu, et al., Tumor-targeted paclitaxel delivery and enhanced penetration using TAT-decorated liposomes comprising redox-responsive poly(ethylene glycol), J. Pharm. Sci. 104 (2015) 1160–1173, https://doi.org/10.1002/jps.24291.
[3] Y. Yang, X. Liu, W. Ma, Q. Xu, G. Chen, Y. Wang, et al., Light-activatable liposomes for repetitive on-demand drug release and immunopotentiation in hypoxic tumor therapy, Biomaterials 265 (2021) 120456, https://doi.org/10.1016/j.biomaterials.2020.120456.
[4] D. Kim, Y. Guo, Z. Zhang, D. Procissi, J. Nicolai, R.A. Omary, et al., Temperature-sensitive magnetic drug carriers for concurrent gemcitabine chemohyperthermia, Adv. Healthc. Mater. 3 (2014) 714–724.
[5] H.C. Besse, A.D. Barten-van Rijbroek, K.M.G. van der Wurff-Jacobs, C. Bos, C.T. W. Moonen, R. Deckers, Tumor drug distribution after local drug delivery by hyperthermia, in vivo, Cancers 11 (2019), https://doi.org/10.3390/cancers11101512.
[6] M.N. Holme, I.A. Fedotenko, D. Abegg, J. Althaus, L. Babel, F. Favarger, et al., Shear-stress sensitive lenticular vesicles for targeted drug delivery, Nat. Nanotechnol. 7 (2012) 536–543, https://doi.org/10.1038/nnano.2012.84.
[7] L. Cruzeiro-Hansson, O.G. Mouritsen, Passive ion permeability of lipid membranes modelled via lipid-domain interfacial area, Biochim. Biophys. Acta Biomembr. 944 (1988) 63–72, https://doi.org/10.1016/0005-2736(88)90316-1.
[8] A. Blicher, K. Wodzinska, M. Fidorra, M. Winterhalter, T. Heimburg, The temperature dependence of lipid membrane permeability, its quantized nature, and the influence of anesthetics, Biophys. J. 96 (2009) 4581–4591, https://doi.org/10.1016/j.bpj.2009.01.062.
[9] H. Ebel, P. Grabitz, T. Heimburg, Enthalpy and volume changes in lipid membranes. I: the proportionality of heat and volume changes in the lipid melting transition and its implication for the elastic constants, J. Phys. Chem. B 105 (2001) 7353–7360, https://doi.org/10.1021/jp010515s.
[10] H. Trauble, H. Eibl, Electrostatic effects on lipid phase transitions: membrane structure and ionic environment, Proc. Natl. Acad. Sci. U. S. A. 71 (1974) 214–219, https://doi.org/10.1073/pnas.71.1.214.
[11] T. Heimburg, The capacitance and electromechanical coupling of lipid membranes close to transitions: the effect of electrostriction, Biophys. J. 103 (2012) 918–929, https://doi.org/10.1016/j.bpj.2012.07.010.
[12] R.A. Böckmann, A. Hac, T. Heimburg, H. Grubmüller, Effect of sodium chloride on a lipid bilayer, Biophys. J. 85 (2003) 1647–1655, https://doi.org/10.1016/S0006-3495(03)74594-9.
[13] K.H. De Haas, C. Blom, D. Van den Ende, M.H.G. Duits, J. Mellema, Deformation of giant lipid bilayer vesicles in shear flow, Phys. Rev. E 56 (1997) 7132.
[14] R. Dimova, K.A. Riske, S. Aranda, N. Bezlyepkina, R.L. Knorr, R. Lipowsky, Giant vesicles in electric fields, Soft Matter 3 (2007) 817–827.
[15] Y.L. Zhang, J.A. Frangos, M. Chachisvilis, Laurdan fluorescence senses mechanical strain in the lipid bilayer membrane, Biochem. Biophys. Res. Commun. 347 (2006) 838–841, https://doi.org/10.1016/j.bbrc.2006.06.152.
[16] T. Parasassi, F. Conti, E. Gratton, Time-resolved fluorescence emission spectra of Laurdan in phospholipid vesicles by multifrequency phase and modulation fluorometry, Cell. Mol. Biol. 32 (1986) 103–108.
[17] T. Parasassi, E. Gratton, Packing of phospholipid vesicles studied by oxygen quenching of Laurdan fluorescence, J. Fluoresc. 2 (1992) 167–174, https://doi.org/10.1007/BF00866931.
[18] T. Parasassi, G. De Stasio, G. Ravagnan, R.M. Rusch, E. Gratton, Quantitation of lipid phases in phospholipid vesicles by the generalized polarization of Laurdan fluorescence, Biophys. J. 60 (1991) 179–189.
[19] M. Bacalum, B. Zorila, M. Radu, Fluorescence spectra decomposition by asymmetric functions: Laurdan spectrum revisited, Anal. Biochem. 440 (2013) 123–129, https://doi.org/10.1016/j.ab.2013.05.031.
[20] M.I. Angelova, S. Soléau, P. Méléard, F. Faucon, P. Bothorel, Preparation of giant vesicles by external AC electric fields, in: C. Helm, M. Lösche, H. Möhwald (Eds.), Kinetics and applications BT - Trends in Colloid and Interface Science VI, 1992, pp. 127–131. Darmstadt: Steinkopff.
[21] T. Heimburg, Thermal Biophysics of Membranes, John Wiley & Sons, 2008.
[22] J. Schindelin, I. Arganda-Carreras, E. Frise, V. Kaynig, M. Longair, T. Pietzsch, et al., Fiji: an open-source platform for biological-image analysis, Nat. Methods 9 (2012) 676–682, https://doi.org/10.1038/nmeth.2019.
[23] S. Preibisch, S. Saalfeld, P. Tomancak, Globally optimal stitching of tiled 3D microscopic image acquisitions, Bioinformatics 25 (2009) 1463–1465, https://doi.org/10.1093/bioinformatics/btp184.
[24] P.J. Davis, K.M.W. Keough, Differential scanning calorimetric studies of aqueous dispersions of mixtures of cholesterol with some mixed-acid and single-acid phosphatidylcholines, Biochemistry 22 (1983) 6334–6340, https://doi.org/10.1021/bi00295a045.
[25] N. Färber, C. Westerhausen, Broad lipid phase transitions in mammalian cell membranes measured by Laurdan fluorescence spectroscopy, Biochim. Biophys. Acta Biomembr. 2022 (1864) 183794, https://doi.org/10.1016/j.bbamem.2021.183794.
[26] B. Wunderlich, C. Leirer, A.-L. Idzko, U.F. Keyser, A. Wixforth, V.M. Myles, et al., Phase-state dependent current fluctuations in pure lipid membranes, Biophys. J. 96 (2009) 4592–4597, https://doi.org/10.1016/j.bpj.2009.02.053.
[27] D. Papahadjopoulos, K. Jacobson, S. Nir, I. Isac, Phase transitions in phospholipid vesicles fluorescence polarization and permeability measurements concerning the

effect of temperature and cholesterol, Biochim. Biophys. Acta Biomembr. 311 (1973) 330–348, https://doi.org/10.1016/0005-2736(73)90314-3.
[28] V.F. Antonov, A.A. Anosov, V.P. Norik, Smirnova Ei, A soft poration of planar bilayer lipid membranes from dipalmitoylphosphatidylcholine at the temperature of the phase transition from the liquid crystalline to the gel state, Biofizika 50 (2005) 867–877.
[29] S.A. Kirsch, R.A. Böckmann, Coupling of membrane nanodomain formation and enhanced electroporation near phase transition, Biophys. J. 116 (2019) 2131–2148, https://doi.org/10.1016/j.bpj.2019.04.024.
[30] T.G. Papaioannou, E.N. Karatzis, M. Vavuranakis, J.P. Lekakis, C. Stefanadis, Assessment of vascular wall shear stress and implications for atherosclerotic disease, Int. J. Cardiol. 113 (2006) 12–18, https://doi.org/10.1016/j.ijcard.2006.03.035.
[31] J. Strony, A. Beaudoin, D. Brands, B. Adelman, Analysis of shear stress and hemodynamic factors in a model of coronary artery stenosis and thrombosis, Am. J. Physiol. Circ. Physiol. 265 (1993) H1787–H1796.